Available online at www.sciencedirect.com

ScienceDirect

materialstoday: PROCEEDINGS

Materials Today: Proceedings 2S (2015) S917 – S920

International Conference on Martensitic Transformations, ICOMAT-2014

In situ synchrotron X-ray diffraction of the martensitic transformation in superelastic Ti-27Nb and NiTi alloys: a comparative study

L. Héraud, P. Castany, D. Laillé, T. Gloriant*

UMR CNRS 6226 Institut Sciences Chimique de Rennes, INSA Rennes, 20 Avenue des Buttes de Coësmes, 35708 Rennes Cedex 7, France

Abstract

In this study, the stress-induced martensitic transformations occurring in superelastic NiTi and Ni free titanium Ti-27Nb alloys were investigated by in situ synchrotron X-ray diffraction analyses during tensile tests. It was observed a direct β to α'' martensitic transformation in the Ti-27Nb alloy while the intermediate R-phase was clearly observed to be stress-induced prior the B19'martensitic phase in the case of the NiTi.

Selection and Peer-review under responsibility of the chairs of the International Conference on Martensitic Transformations 2014.

Keywords: In situ synchrotron; X-ray diffraction; NiTi; Titanium alloy; Stress-induced martensitic transformation

1. Introduction

The intermetallic NiTi is largely used in the biomedical field [1] because of its excellent mechanical properties, particularly its very high recoverable strain. Its superelastic property is due to the stress-induced martensitic transformation (SIM) between the B2 austenitic phase (cubic, space group $Pm\bar{3}m$), and the B19' martensitic phase (monoclinic, space group $P2_1/m$). This transformation remains however still complex and it can be occasionally observed the occurrence of a transitional phase: the R-phase [2]. Gorycka et al. demonstrated that the R-phase is

* Corresponding author. Tel.: +33-223-238-241; fax: +33 223-238-240.
E-mail address: thierry.gloriant@insa-rennes.fr

Selection and Peer-review under responsibility of the chairs of the International Conference on Martensitic Transformations 2014.
doi:10.1016/j.matpr.2015.07.431

trigonal (space group $P\bar{3}$) [3, 4] but the space group of this phase is still subject to controversy. This can be due to the fact that the martensitic transformation in NiTi was characterized mainly under thermal cycling from shape memory NiTi [5]. On the other hand, the studies concerning the SIM transformation in superelastic NiTi under synchrotron radiation mentioning the presence of R-phase are few [6].

For biomedical applications, there is a need to develop Ni free alloys showing superelastic properties as the nickel is known to be strongly allergenic in some cases [7]. Highly biocompatible metastable β titanium alloys such as TiNb based alloys are then promising candidates to replace NiTi for certain biomedical devices [8,9]. In metastable β Ti-alloys, the superelastic property is the consequence of the SIM transformation occurring between the austenitic β phase (body centered cubic structure, space group $Im\bar{3}m$) and the stress-induced martensitic α'' phase (C-centered orthorhombic, space group Cmcm).

The aim of this work is to compare the characteristics of the SIM transformations taking place in NiTi and Ti-27Nb alloys by synchrotron X-ray diffraction (SXRD). To achieve this purpose, in situ cyclic loading/unloading tensile tests under synchrotron radiation were carried out. Diffraction patterns were collected for each cycle in order to determine the involved phases and to characterize the evolution of the lattice parameters.

2. Materials and methods

In this study, the binary Ti-27Nb (at %) alloy was synthesized by the cold crucible levitation melting technique. For the synthesis, ultra-pure raw metals: 99.999% pure titanium and 99.9% pure niobium were used. The ingot was homogenised at 1223K for 72ks and quenched in water. It was then cold rolled to 0.4 mm thick sheets and machined into normalized tensile specimens (3 mm width and a gage length of 15 mm). It was finally solution treated at 1123K for 1.8ks and water quenched to ensure a fully β state. The NiTi samples were purchased from Alfa Aesar in sheets of 0,38 mm in thickness, with a composition of 55,8%wt of Ni and 44,2%wt of Ti. The normalized tensile specimens were cut by electric discharge machining from the sheets.

The in situ SXRD characterizations were carried out at the European Synchrotron Radiation Facility (ESRF) in Grenoble, France, with the high resolution beam line ID31. The incident wavelength was 0.400021 nm and data collection was performed in transmission at room temperature over the 2θ angular range 8–20° with a step size of 0.005°. A tensile test device was positioned in front of the beam. The cyclic loading/unloading tensile tests consist here to apply a succession of incremental tensile strains that are all followed by unloading to release the stress. For NiTi, the tensile strain was incremented by 1% up to 12%. In the case of the Ti-27Nb alloy, the tensile strain was incremented by 0.5% up to 6% and by 2% up to 10%. Diffraction patterns were recorded for each cycle on loading and after each unloading. Analysis of the diffraction data consisted in identifying the different phases and then calculating their lattice parameters.

3. Results and discussion

Figure 1 shows the cyclic stress-strain curves related to each alloy, NiTi (a) and Ti-27Nb (b). Both curves present the typical double yielding behaviour associated with a stress plateau due to the reversible SIM transformation occurring between the austenite and the martensite. As observed, the plateau is about 4% long and 1.5 % long (in strain) for NiTi and Ti-27Nb, respectively. These values are in good agreement with those found in literature [1-2, 8-9]. Above 6% and 2% of deformation for NiTi and Ti-27Nb respectively, the SIM transformation is nearly achieved; further strain is then mainly accommodated by the elastic deformation of the martensite. The recovery strain of the NiTi is total up to 10% of deformation. By comparison, the recovery strain of the Ti-27Nb is total only up to 2%.

The SXRD patterns for different strain levels under loading and after each unloading are presented in Figs. 2a and b for NiTi and in Figs. 2c and d for Ti-27Nb, respectively. The SRXD pattern of NiTi in the initial state is well indexed by the B2 austenitic phase. When the strain rises, the B2 austenite peaks intensities are decreasing and some other peaks appear. These additional peaks, appearing from 1% strain, do not correspond to B19' martensite but can be very well indexed with the transitional R-phase. Moreover the occurrence of this phase is consistent with the tensile curve, where a change in slope can be observed in the elastic deformation portion of the austenite in the tensile curve [6]. The relative intensity of the R-phase peaks increases until that the B19' martensite's more intense peak, $(110)_{B19'}$, starts to appear at 2 % strain, which corresponds to the beginning of the plateau on the tensile curve.

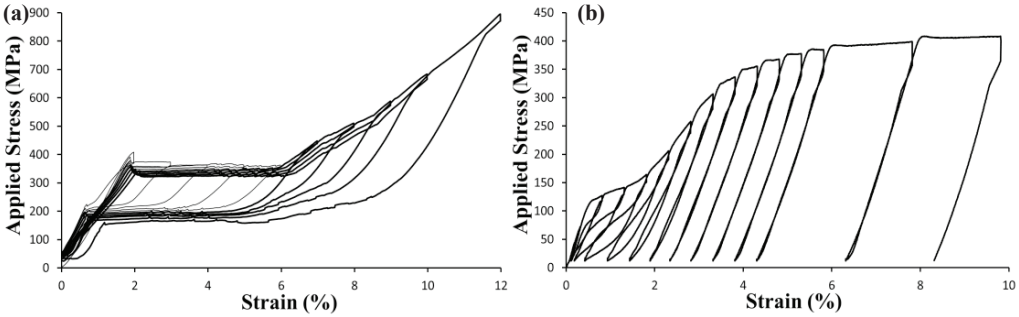

Fig. 1. Cyclic tensile tests of TiNi (a) and Ti-27Nb (b) carried out during in situ synchrotron X-ray diffraction.

It is worth noting that the R-phase coexists with both martensitic B19' and austenitic B2 phases up to 4% strain before completely disappearing. From about 6% of deformation, the NiTi is mainly martensitic. Along the plateau, the martensite peaks are growing while the austenite peaks are decreasing until disappearing. It can be observed that all the SXRD diffractograms obtained after each unloading only display the peaks related to the B2 austenitic phase. That means that the stress-induced R-phase is also reversible as well as the B19' phase.

Concerning the other alloy, the intense $(110)_\beta$ peak confirms that the Ti-27Nb alloy is fully β at the initial state. Under loading, the α'' SIM transformation is observed without the presence of an intermediate phase. This transformation is highlighted by the fact that the intensity of the $(110)_\beta$ peak is decreasing gradually upon deformation while the $(020)_{\alpha''}$ peak is appearing. For both alloys the reversibility of the SIM transformation is shown by the relative increase of the austenitic peak after unloading with respect to the corresponding loading level. Thus, it is confirmed by SXRD that a complete reversibility is still obtained up to 10% of strain for NiTi and only below 2% for Ti-27Nb.

From the different SXRD patterns obtained, the evolutions of cell parameters for the different phases were plotted as a function of the deformation percentage under loading. Figure 3a shows changes in the lattice parameters of the B2 phase (a_{B2}), the R-phase (a_R, c_R) and the B19' phase ($a_{B19'}$, $b_{B19'}$, $c_{B19'}$, $\gamma_{B19'}$) of the NiTi. Figure 3b shows the evolution of the β phase (a_β) and the α'' phase ($a_{\alpha''}$, $b_{\alpha''}$ and $c_{\alpha''}$) parameters of the Ti-27Nb. The parameter a_{B2} of the NiTi's austenite increases rapidly to 2% and then remains more or less constant up to 4% where it is no longer indexable. Concerning the R-phase, a strong decrease of the a_R is observed on straining. The lattice parameters of the B19' martensite could not be obtained properly before 4% strain, since there were not enough peaks. Up to around 5-6% of strain, $a_{B19'}$, $b_{B19'}$ and $\gamma_{B19'}$ decrease and $c_{B19'}$ increases. Above 6% of deformation, all B19' martensite cell parameters increase reflecting that this is the elastic deformation of the martensite that accommodates the deformation after the SIM plateau.

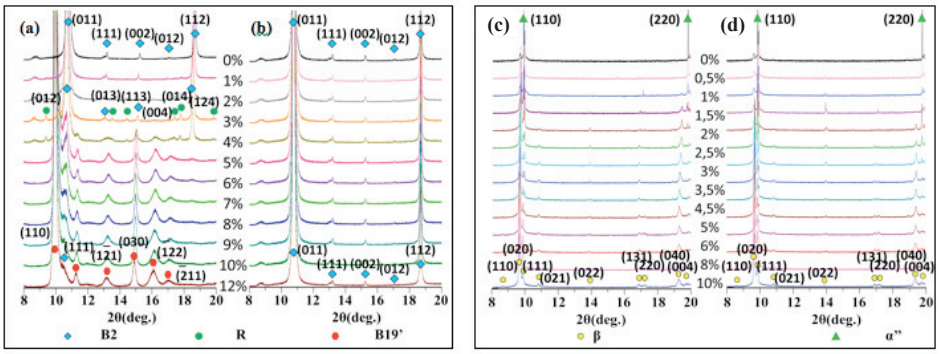

Fig. 2. SXRD patterns corresponding to the different incremental strain % under loading (a) and after each unloading (b) for NiTi. SXRD patterns corresponding to the different incremental strain % under loading (c) and after each unloading (d) for Ti-27Nb.

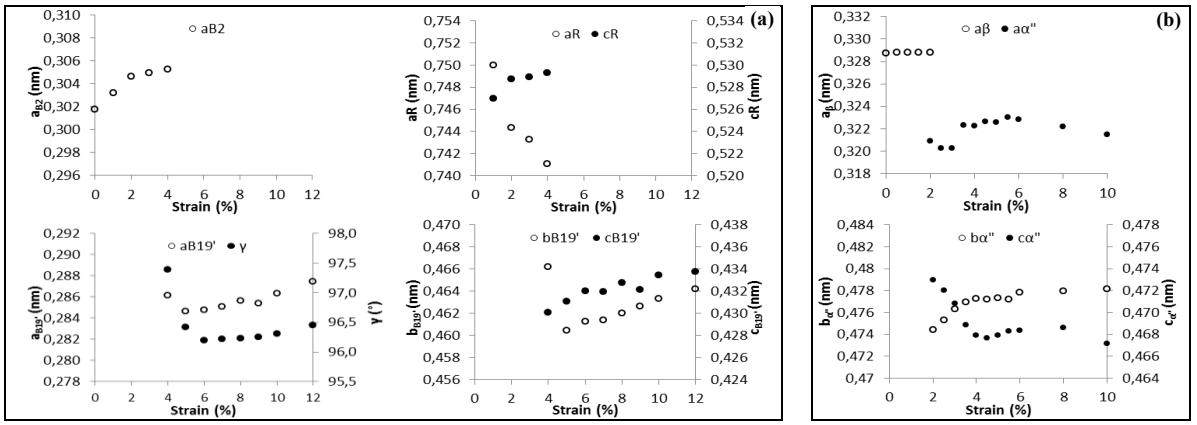

Fig. 3. a) Evolution of lattice parameters of B2, R and B19' phases as a function of the applied strain during in situ tensile tests for NiTi. b) Evolution of lattice parameters of β and α" phases for Ti-27Nb.

Figure 3b shows that the β cell parameter (a_β) of the Ti-27Nb alloy remains essentially constant, the deformation being accommodated by the martensitic transformation that occurs quickly at about 0.5% of strain. It can be noted that although the martensitic transformation is already detected after 0.5% of strain (see tensile curve in Fig. 1.), the cell parameters cannot be evaluated precisely before 2% deformation. Between 2 and 3.5% strain, the parameter $a_{\alpha''}$ seems stable at about 0.320 nm; at 4% strain it undergoes a sharp increase before oscillating around 0.323 nm. Between 2 and 4% deformation the parameter $b_{\alpha''}$ increases from 0.474 to 0.477 nm and the parameter $c_{\alpha''}$ decreases from 0.473 to 0.467 nm. Above 4% strain $b_{\alpha''}$ and $c_{\alpha''}$ continue to vary more slowly toward stabilization. All those observations indicate that the deformation of the Ti-27Nb after the plateau is accommodated firstly by elastic deformation of the martensite and then by its plastic deformation, as observed on the tensile curve (Fig. 1).

4. Conclusion

In this study, we showed that SIM transformations can be clearly characterized by in situ SXRD analyses under loading/unloading tensile tests. The relative evolution of all austenitic and martensitic phases was observed during the reversible SIM transformation intervening in both NiTi and Ti-27Nb alloys. In the superelastic NiTi alloy, the intermediate R-phase is firstly stress-induced from about 1% of strain prior to the B19' martensitic phase, which starts at about 2% of strain at the beginning of the stress plateau. We showed that both martensitic R-phase and B19' phase transformations are reversible after unloading. On the contrary, the Ti-27Nb alloy does not present transitional phase and a direct β into α'' reversible stress-induced martensitic transformation was observed.

Acknowledgements

We acknowledge the European Synchrotron Radiation Facility for provision of synchrotron radiation facilities and we would like to thank Yves Watier for assistance in using beamline ID31.

References

[1] T. Duerig, A. Pelton, D. Stockel, Mater. Sci. Eng. A 273–275 (1999) 149–160.
[2] K. Otsuka, X. Ren, Prog. Mater. Sci. 50 (2005) 511–678.
[3] T. Goryczka, H. Morawiee, J. Alloys Compd. 367 (2004) 137–141.
[4] J. Khalil-Allafi, W.W. Schmahl, D.M. Toebbens, Acta Mater. 54 (2006) 3171–3175.
[5] N.G. Jones, D. Dye, Intermetallics 19 (2011) 1348–1358.
[6] M.L.Young, M.F.-X. Wagner, J. Frenzel, W.W. Schmahl, G. Eggeler, Acta Mater. 58 (2010) 2344–2354.
[7] S.A. Shabalovskaya, Bio-Med. Mater. Eng., 12 (2002) 69-109.
[8] H.Y. Kim, Y. Ikehara, J.I. Kim, H. Hosoda, S. Miyazaki, Acta Mater. 54 (2006) 2419–2429.
[9] E. Bertrand, P. Castany, T. Gloriant, Acta Mater. 61 (2013). 511–518.